Chem. Senses 32: 273–284, 2007

doi:10.1093/chemse/bjl056
Advance Access publication January 13, 2007

Numerical Modeling of Odorant Uptake in the Rat Nasal Cavity

Geoffrey C. Yang[1,2], Peter W. Scherer[1], Kai Zhao[1] and Maxwell M. Mozell[3]

[1]Department of Bioengineering, School of Engineering and Applied Science, University of Pennsylvania, Philadelphia, PA 19104, USA and [3]Department of Neuroscience and Physiology, State University of New York, Upstate Medical University, Syracuse, NY 13210, USA
[2]Present address: Affymetrix, Inc., 3420 Central Expressway, Santa Clara, CA 95051, USA

Correspondence to be sent to: Peter W. Scherer, Department of Bioengineering, School of Engineering and Applied Science, University of Pennsylvania, 240 Skirkanich Hall/6321, 210 South 33rd Street, Philadelphia, PA 19104, USA. e-mail: scherer@seas.upenn.edu

Abstract

An anatomically accurate 3-dimensional numerical model of the right rat nasal cavity was developed and used to compute low, medium, and high flow rate inspiratory and expiratory mucosal odorant uptake (imposed patterning) for 3 odorants with different mucus solubilities. The computed surface mass flux distributions were compared with anatomic receptor gene expression zones identified in the literature. In general, simulations predicted that odorants that were highly soluble in mucus were absorbed dorsally and medially, corresponding roughly to receptors from one of the gene expression zones. Insoluble odorants tended to be absorbed more peripherally in the rat olfactory region corresponding to the other 2 zones. These findings also agreed in general with the electroolfactogram measurements and the voltage-sensitive dye measurements reported in the literature. This numerical approach is the first to predict detailed odorant flux information across the olfactory mucosa in the rat nasal cavity during inspiratory and expiratory flow and to relate it to anatomic olfactory receptor location, physiological function, and biochemical experiment. This numerical technique can allow us to separate the contributions of imposed and inherent patterning mechanisms on the rat olfactory mucosa.

Key words: absorption, finite element analysis, mucus solubility, nasal fluid mechanics, odorant flow rate, receptor gene expression zones

Introduction

In the rat nose, odorant molecules travel through and are absorbed along a long multichannel path lined with nonolfactory mucosa before reaching the olfactory epithelium, some of which lies in the blind ethmoid recesses of the ethmoturbinates. The molecules in the airflow reaching the olfactory region are absorbed onto the surface of the mucosa and diffuse through its depth to reach the olfactory receptors. The entire process consists of convective–diffusive transport of odorant molecules from the ambient air to the surface of the mucus layer, diffusion through the mucus layer, potential transport via chemical reactions with molecules in the mucus, and contact with the olfactory receptors. Next, the receptor cell activity cascade is excited and, finally, odorants are removed from the mucosa which, under the conditions of the current study, is assumed to occur via the vascular supply. Several physicochemical variables, including the diffusivity of the odorant molecules in the air and mucus phases, the solubility of the odorant molecules in the mucus, and the velocity field of the nasal airflow, are involved in the temporal and spatial distribution of the molecules to the receptors.

In this regard, Adrian (1950), in order to explain the different odorant-dependent spatiotemporal patterns of discharge magnitudes and latencies recorded in the olfactory bulb, postulated the existence of parallel antecedent odorant-dependent spatiotemporal patterns of neural activity at the level of the olfactory mucosa which would differ in accordance with each odorant's value of some physicochemical property. Using a variety of techniques, Mozell et al. (1987, 1991) later showed that different odorants flowing across the mucosa do, indeed, produce different spatiotemporal patterns of neural activity and that these differences are related to the strength with which an odorant's molecules are absorbed to the mucosa in a process analogous to gas chromatography. That is, in a given inspiration, the molecules of some odorants moving along the mucosal flow path reached the receptors farther downstream, more rapidly, and in greater numbers than the molecules of other odorants.

When, instead of allowing the odorants to flow across the mucosa, the odorants were puffed directly down onto it at circumscribed locations (Kauer and Moulton 1974; Mackay-Sim et al. 1982), maximal electrophysiologically recorded responses were elicited by different odorants at different locations on the mucosa. These results demonstrated that different odorants can establish spatially different activity patterns across the mucosa without the flow and differential sorption process described by Mozell. Indeed, it was thought that these differential activity patterns evoked by localized puffs would be generated by a very different process based upon differing mucosal positions for olfactory receptor types having different odorant selectivities. That is, all the receptors of a particular type that are tuned to the same chemical or chemical ligand would be primarily aggregated to the same mucosal regions, and each receptor type would have its own spatial pattern of aggregations.

For many years, the idea that aggregates of different types of olfactory receptors were distributed on the mucosa in different patterns was primarily indicated by electrophysiological evidence, but during the past decade, this idea has been confirmed by a number of anatomical studies using the more direct and powerful cell and molecular techniques now available. Several investigators (Ressler et al. 1993; Vassar et al. 1993; Strotmann et al. 1994; Sullivan et al. 1996) have identified up to 4 biochemically separable receptor gene expression zones extending anterior–posteriorly throughout the olfactory mucosa in rodents. These zones have also been reported to be distributed with overlapping boundaries (Iwema et al. 2004; Miyamichi et al. 2005). Some of these circumscribed receptor zones, identified (Strotmann et al. 1994) and referred to in this paper, include the dorsal zone in Strotmann et al. (1994) (or zone 1 in Sullivan et al. 1996), the medial zone (zone 2), and the lateral zone (zone 3). Note that zone numbers will be referred to frequently, as they were defined in the terminology of Sullivan et al. (1996).

Moulton (1976), noting that the data appeared to show at least 2 mechanisms for differential odorant-induced mucosal activity patterns, referred to those patterns based upon the spatial distribution of selectively tuned receptors as ''inherent'' patterns and those dependent upon the differential distribution of the odorant molecules along the mucosal flow path as ''imposed'' patterns. Thus, as the molecules of different inspired odorants pass over the olfactory mucosa during normal smelling, they could simultaneously generate both different imposed and inherent activity patterns (due to the differences in the location of the receptors tuned to them). The recorded result of the interaction between the imposed and inherent activity patterns was called ''composite'' activity patterns by Kent et al. (Kent and Mozell 1992; Kent et al. 1996).

Employing the voltage-sensitive dye technique, Kent et al. (1996) studied the relationship among imposed, inherent, and composite activity patterns. They recorded inherent activity patterns produced by puffing 3 different odorants with varying mucosal sorption strengths directly and uniformly onto the mucosa. They also recorded composite activity patterns produced by the same odorants drawn along the mucosal flow path at 3 different flow rates. Subtraction of the inherent patterns from the composite patterns gave the imposed patterns, and all 3 patterns were compared. The authors observed that the imposed patterns became more dominant as the mucosal sorption of the odorants increased and, conversely, the inherent patterns became more dominant as the mucosal sorption of the odorants decreased. Furthermore, they observed that increasing the odorant flow rate across the mucosa decreased the magnitude of the imposed pattern.

To investigate the effects of airflow rate and odorant physiochemical properties on imposed odorant patterning, we have constructed a 3-dimensional (3D) anatomically accurate finite element model of the right nasal cavity of the Sprague-Dawley rat based on digitization of photomicrographs of nasal cast sections. Both simulated inspiration and expiration under 3 different physiological flow rates characteristics of resting breathing and sniffing were investigated (Yang 1999; Zhao et al. 2004, 2006; and the accompanying paper, Yang et al. 2006). In the present study, we computed the total odorant uptake and the regional mucosal surface mass flux patterns (especially in the olfactory region) of 3 different odorant molecules, for both inspiratory and expiratory flow. Simulated flux variations were caused by a combination of nasal airflow rate and local velocity, odorant diffusivity in air and mucus phases, and odorant mucus solubility. This numerical technique can allow us to separate the contributions of imposed and inherent patterning mechanisms on the rat olfactory mucosa by relating anatomic olfactory receptor location, physiological function, and biochemical experiment to numerical odorant flow and transport data.

Materials and methods

A 3D anatomically accurate model of the right Sprague-Dawley rat nasal cavity was developed with details in the accompanying paper (Yang et al. 2006) and also in the previous works of Yang (1999) and Zhao et al. (2004, 2006). For easier comparison with results from the literature, coronal planes were numbered and compared with Strotmann's sections (Strotmann et al. 1994; Figure 1; Table 1). Throughout the paper, our numbering system will be used unless otherwise specified.

Governing equations and boundary conditions

The governing equations for the steady-state transport of odorant molecules in the gas phase are the Navier–Stokes, continuity, and convective–diffusion equations. The first 2 sets of equations represent transport by respiratory airflow and were described in the accompanying paper (Yang et al. 2006) and also in the previous works of Yang (1999) and Zhao et al. (2006). The steady-state convective–diffusion equation is

Figure 1 Diagrammatic coronal nasal cavity sections (numbering from anterior to posterior) defined by Strotmann et al. (1994) through the right rat olfactory region. The airway is shown in black and the bony septum is to the left of each coronal section. Ours along with Strotmann's numbering are labeled on the sections.

Table 1 Comparison of the numbering system of the coronal sections

Coronal section ID		Distance (cm)[a]
Yang (1999)	Kimbell et al. (1997)	
126	*K*6	1.58
149		1.86
163		2.04
176		2.2
188		2.35
200	*K*23	2.5
226		2.83
241		3.01

[a]Distance is calculated from the anterior tip of nose to each section.

$$u\nabla c = D_a \nabla^2 c, \tag{1}$$

where c is the odorant mass concentration (in air) nondimensionalized by the inlet odorant concentration C_0, u is the air velocity vector, D_a is the odorant air-phase diffusivity, and ∇ and ∇^2 are the gradient and Laplace operators, respectively. The concentration of odorant in the inhaled air was assumed low enough that the physical properties of the air were not affected, and the convective–diffusion equation was decoupled from the airflow equations.

The boundary conditions during simulation of inspiratory and expiratory flows for the first 2 sets of equations (Navier–Stokes and continuity equations) have been detailed in the accompanying paper (Yang et al. 2006) and also in the previous works of Yang (1999) and Zhao et al. (2006). Unsteadiness in the flow field was neglected because the Strouhal number N_{St} is much less than unity for the rat nasal airflow and a quasi-steady boundary layer in the airway can be established.

A mixed, air-phase, wall concentration boundary condition as used by Keyhani et al. (1997) was applied at the air–mucosal wall interface to simulate odorant uptake during respiration (Figure 2). Uniform thickness and composition of the mucus layer throughout the posterior rat nasal cavity were assumed. The air–mucosal wall boundary condition included absorption of odorants from ambient air into the olfactory mucus layer, diffusion of odorants across the mucus layer, and removal of odorants by the submucosal blood flow where the concentration at the mucus/tissue interface was set equal to zero ($c = 0$) for the odorant. The nondimensional steady-state air–mucosal surface boundary condition is given by (Keyhani et al. 1997)

$$\frac{\partial c_w}{\partial y} + Kc_w = 0, \tag{2}$$

where c_w is odorant concentration at the air–mucosal surface, y is the coordinate in the direction perpendicular to the air–mucosal surface, and the nondimensional wall surface parameter K is given by $K = \frac{d_{in} D_m}{D_a \beta H_m}$, where d_{in} is the hydraulic diameter (= 4 × area/perimeter) of the external naris, D_m and D_a are the diffusivity of inhaled odorant in the mucus and air phases, respectively, β is the odorant partition coefficient at the air–mucus interface, and H_m is the thickness of the mucus layer (assumed to be uniform at 30 μm; Getchell et al. 1984). This is an estimated value but consistent with assuming uniform mucus thickness. The thickness is the level where all odorant are assumed removed by capillary blood and which includes some tissue where the capillaries are embedded. We used all odorant parameter values exactly as used by Keyhani et al. (1997). Specifically, we are using the same values of solubility for carvone (C), amyl acetate (AC), and octane as used in Keyhani et al. (1997), which are based on experimental measurements on bullfrogs by Hornung et al. (1980, 1987) and Hornung and Mozell (1981). These β values are also listed in Table 2.

In all, odorant uptake for quasi-steady transport in the nasal cavity can be characterized by 3 independent nondimensional parameters—the Reynolds number $N_{Re} = \frac{U_{in} d_{in}}{\nu}$, the Schmidt number $N_{Sc} = \frac{\nu}{D_a}$, and wall surface parameter K, where ν is the kinematic viscosity of air. Two limiting cases can be described for the parameter K: a highly mucus soluble odorant ($\beta \to 0, K \to \infty, c_w = 0$) and a highly insoluble odorant $\left(\beta \to \infty, K \to 0, \frac{\partial c_w}{\partial y} = 0\right)$.

The anterior end of the rat nose, which is lined by stratified squamous epithelium, was simulated as impermeable to odorants, and a boundary condition of zero-wall mass flux $\left(K \to 0, \frac{\partial c_w}{\partial y} = 0\right)$ was applied. Figure 6 in the Results will demonstrate the no-wall flux region in the anterior end of the nose.

A constant and uniform dimensionless concentration boundary condition of c = 1.0 was imposed at the inlet for all inspiratory simulations. At the end section of the nasopharyngeal meatus (outlet), the normal derivative of concentration was set equal to zero (zero normal diffusive flux)

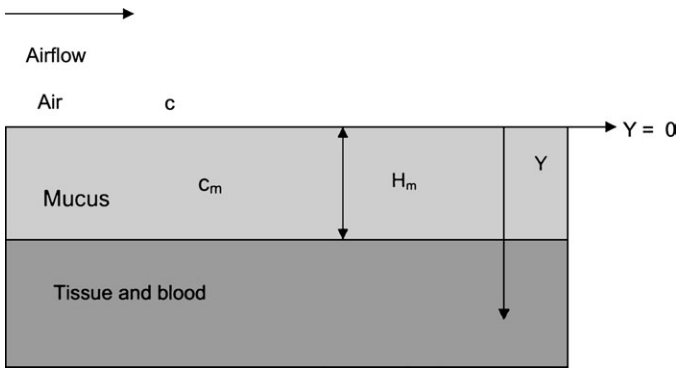

Figure 2 A diagrammatic representation of the mass transfer boundary condition at the air–mucosa interface as used by Keyhani et al. (1997). Symbols are as defined in the Appendix.

because the diffusive flux is much smaller than the convective flux at the high airflow rates present there. For simulated steady-state expiratory flow, a uniform concentration profile (c = 1.0) was applied at the nasopharyngeal meatus (inlet), and zero normal flux was imposed at the outlet.

Computation of wall flux

The concentration of odorant molecules throughout the lumen of the nasal cavity was approximated by solving the convective–diffusion equation with the boundary conditions noted above. The normal component of mass flux (g/cm^2/s) at any node on the wall surface of the 3D mesh is expressed in the form

$$j_n = -D_a \left.\frac{\partial c_a}{\partial y}\right|_{wall}. \quad (3)$$

The total odorant flow, J (g/s), over a given wall surface is then determined by integrating j_n's over the area of the wall surface, A. The absorption efficiency η of the entire nose is defined as the total odorant uptake over the wall surface area divided by the total inlet odorant mass flow.

Strotmann et al. (1994) used 20 coronal sections to study the distribution of different receptor gene expression zones in the rat nasal olfactory region. From these, 4 coronal sections (2 anterior to and 2 in the ethmoid recesses; labeled as sections S4, S7, S13, and S16) were selected for our study, and the wall fluxes on these olfactory surfaces were computed (see Results). These planes were equivalent to coronal planes 163, 176, 200, and 226, respectively, in our numbering system (Table 1). Planes 163 and 176 were located relatively anteriorly in the olfactory region and contained less turbinate structure, whereas planes 200 and 226 were located in the posterior end with most of the nasal walls overlaid by olfactory epithelium.

Surface odorant uptake for inspiratory and expiratory flow was computed for 3 different odorants—very mucus soluble C, intermediately soluble AC, and highly insoluble octane. The same physiological half-nasal flow rates (126, 252, and 504 ml/min) used to study the velocity field in the rat nasal cavity were used to solve the convective–diffusion equation for the concentration field throughout the nasal cavity.

Vector plots of mass flux on the nasal walls of these coronal planes showed the local distribution and magnitude of the odorant uptake during inspiratory and expiratory flow. All surface fluxes were normalized by the inhaled odorant mass fraction C_0/ρ, where ρ is the density of air (1.177×10^{-3} g/cm^3), allowing us to represent odorant flux independent of ambient odorant concentration. To recover the actual odorant flux in a given case, it is necessary to multiply the given values by the inhaled odorant mass fraction.

Numerical solution methods

The velocity field solution to the Navier–Stokes and continuity equations obtained in the accompanying paper (Yang et al. 2006) and also in the previous works of Yang (1999) and Zhao et al. (2006) was used to solve the uncoupled convective–diffusion equation. The convergence criterion used for the termination of concentration iterations required that the norm of nodal concentration differences between iterations be less than 10^{-3}, that is

$$\frac{\|c_i - c_{i-1}\|}{\|c_i\|} \le \text{tolerance}(=0.1\%), \quad (4)$$

where c_i is the concentration solution vector at iteration i and $\|\cdot\|$ is the root mean square norm summed over all the nodes of the model.

At all values of N_{Re}, N_{Sc}, and K, converged concentration fields were reached within 400 iterations, depending on the mucus solubility of the odorants, requiring approximately 6 min of central processing unit time for each iteration. Conservation of species mass in the model was checked for the final solution to the convective–diffusion equation. The difference between the odorant mass entering the inlet and exiting the nasopharyngeal meatus over a given time should be equal to the total absorption on the nasal mucosal wall during that time. In general, an error of less than 0.9% for all values of N_{Re}, N_{Sc}, and K was found. A mesh size convergence test was also applied by increasing the number of nodes by a factor of 10 and noting negligible difference in the values c_i's.

Results

This paper, as well as the accompanying paper (Yang et al. 2006) and also in the previous works of Yang (1999) and Zhao et al. (2006), demonstrates numerically simulated, not measured results in the nasal cavity. All odorant uptake results without further specification come from the numerical modeling research utilizing the computational fluid dynamics techniques.

Predicted surface odorant flux patterns (Figure 3A–F) were found to vary significantly among the 3 odorants

Table 2 Chemical structure versus physical properties of a number of odorants (at 25 °C and 1 atm)

Odorants[a]	Solubility	D_a (cm^2/s)	$D_m \times 10^5$ (cm^2/s)[b]	β air/water partition coefficient[c]	Functional group
C	High	0.062[d]	0.69[e]	1.30×10^{-4} [f]	Ketone
Menthone				4.44×10^{-3} [g]	
AC	Intermediate	0.067[d]	0.78[e]	2.50×10^{-3} [h]	Bicyclic
1,8-Cineole				4.46×10^{-3} [g]	
Fenchone				2.84×10^{-3} [g]	
7-Oxabicycloheptane				3.65×10^{-2} [g]	
***n*-Octane**	Low	0.060[i]	0.7[e]	4.8×10^{-1} [j]	Lack oxygen
Limonene				8.14×10^{-1} [g]	
α-Terpinene				4.46×10^{-1} [g]	
α-Pinene				4.33[g]	

Note that odorants are not sorted by their absolute partition coefficients; instead, they are tabulated and grouped into functional groups.
[a]Odorants used by Scott et al. (1996, 1997); odorants in this study are bold-faced.
[b]Values in water.
[c]Air–water interface values unless otherwise noted.
[d]Calculated using the Fuller equation (Welty et al. 1976).
[e]Calculated using the Wilke–Chang equation (Welty et al. 1976).
[f]Hornung et al. (1980), air/bullfrog nasal mucosa partition coefficients.
[g]Howard et al. (1997).
[h]Hornung et al. (1987), air/bullfrog nasal mucosa partition coefficients.
[i]Welty et al. (1976).
[j]Hornung and Mozell (1981), air/bullfrog nasal mucosa partition value.

studied. Generally, C was strongly absorbed onto the mucosal surface upstream for both inspiratory and expiratory flow, whereas absorption of octane was predicted to be more even throughout the cavity for both flow directions.

Wall flux on the olfactory surface

Simulated wall flux predicted that C was strongly absorbed onto the olfactory mucosal surface dorsomedially especially during expiration, whereas octane was more peripherally absorbed throughout the cavity with small amounts of absorption for both inspiratory and expiratory flow. Simulated AC tended to be absorbed on the nasal walls of the 4 coronal sections at similar locations to C but with considerably smaller magnitudes of mass surface flux than C. These AC and C locations lay on both lateral and medial walls of the middle–ventral region of the main meatus and on the exterior surface of the nasopharyngeal meatus. Another major location predicted for C and AC absorption lay in the most dorsal (dorsomedial) region of the main meatus. The locations for octane absorption tended to move toward the more lateral meati and on the junctions between the lateral and main meati.

Because the 4 coronal sections were downstream (from the inlet) on the flow path during inspiratory flow, increasing mass surface flux with increasing airflow rate was predicted for all 4 sections as expected (see Discussion). The predicted effect of increasing flow rate also varied with the mucus solubility of the odorants; that is, C absorption increased greatly on all 4 coronal sections when the flow rate was increased from 126 to 504 ml/min. Absorption of AC increased somewhat, whereas octane absorption changed very little.

Higher mass surface flux was simulated for all odorants on these 4 coronal sections for expiratory flow than for inspiratory flow because during expiratory flow, the sections are located upstream near the $c = 1$ boundary condition at the flow inlet. However, most of the predicted increase occurred near the septum rather than near the turbinates. The magnitude of mass surface flux for C absorption was predicted to be increased by between 4 and 7 times (depending on the 3 flow rates) as the flow direction was reversed. Increases in the mass fluxes were also predicted for AC and octane during expiratory flow compared with inspiratory flow.

Total uptake of odorants

Total inspiratory odorant uptake was predicted for the entire rat nasal mucosa. As flow rate increased, simulated total mass surface flux for all 3 odorants increased, with sharp rises in the total flux for C (~190% increase from the low flow rate to the high flow rate) and AC (90%) and a relatively mild rise for octane (35%) during inspiration (Figure 4). A similar effect was predicted for expiratory flow. Unlike total odorant surface flow, absorption efficiency η decreases for all 3 odorants as the flow rate increases for both flow directions (Figure 5).

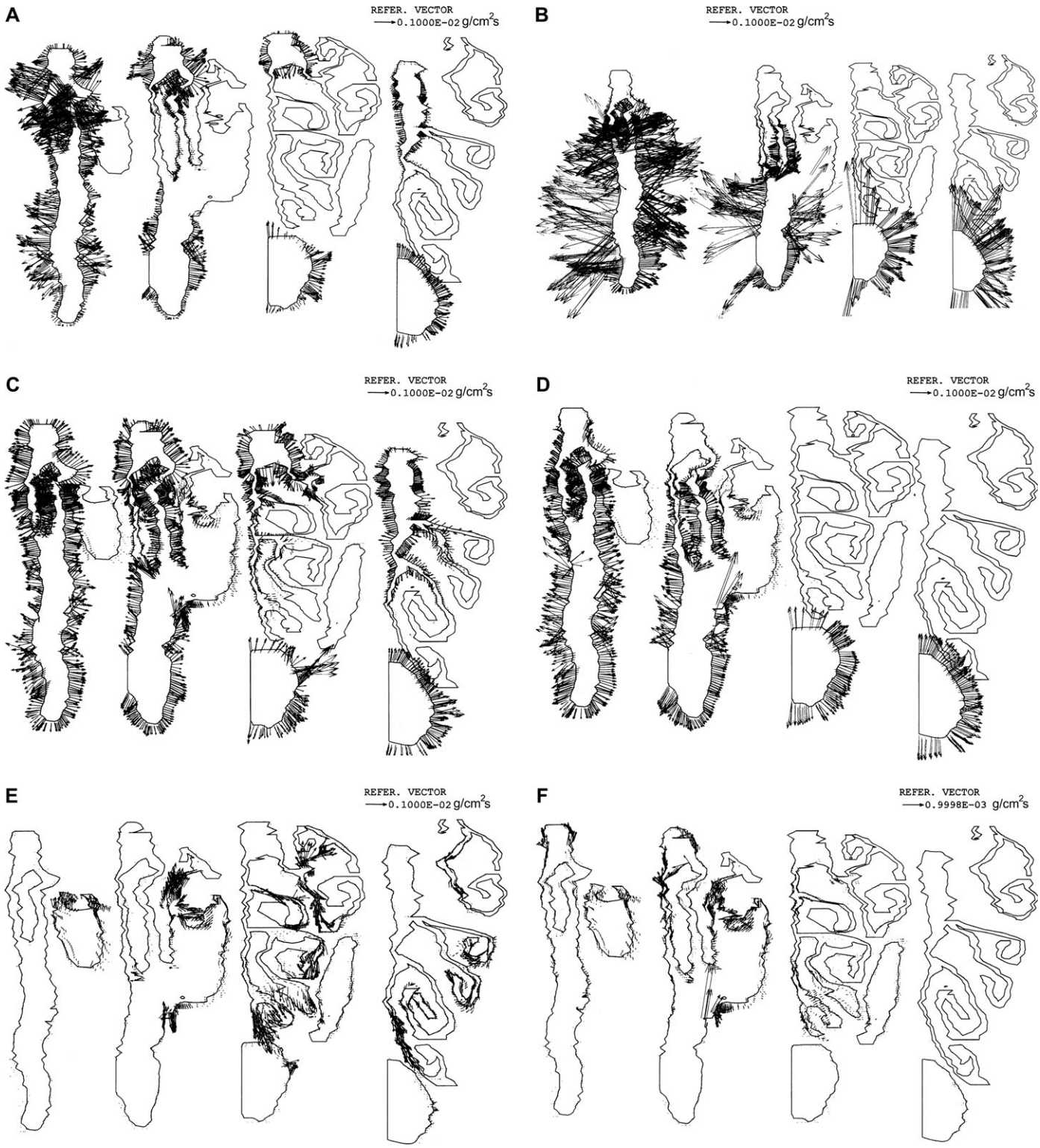

Figure 3 Vector plots of the surface mass flux absorption for 3 odorants on 4 coronal sections (163, 176, 200, and 226; left to right) at half-nasal flow rate of 504 ml/min. Reference unit vector is 1×10^{-3} g/cm^2/s. **(A)** C at inspiratory flow, **(B)** C at expiratory flow, **(C)** AC at inspiratory flow, **(D)** AC at expiratory flow, **(E)** Octane at inspiratory flow, and **(F)** Octane at expiratory flow. During inspiratory and expiratory flow, the direction of the airflow is out of the paper and into the paper, respectively. The length of the vectors shows the absolute magnitude of the (air) surface flux at the specific normal surface and is assigned according to the scale shown. The direction of the arrow points outward normal to the local surface area.

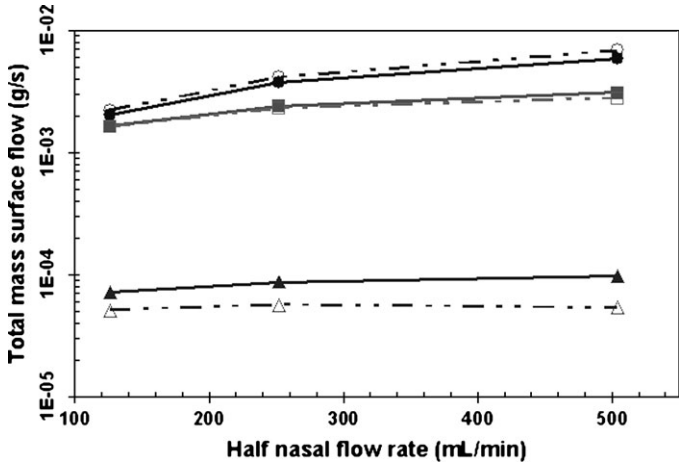

Figure 4 Total odorant surface flow onto the entire nasal surface (g/s) normalized by the mass fraction at the inlet, plotted against half-nasal flow rate $Q_{/2}$. Key: C (●/○), AC (■/□), octane (▲/Δ), inspiratory flow (solid lines), and expiratory flow (dashed lines).

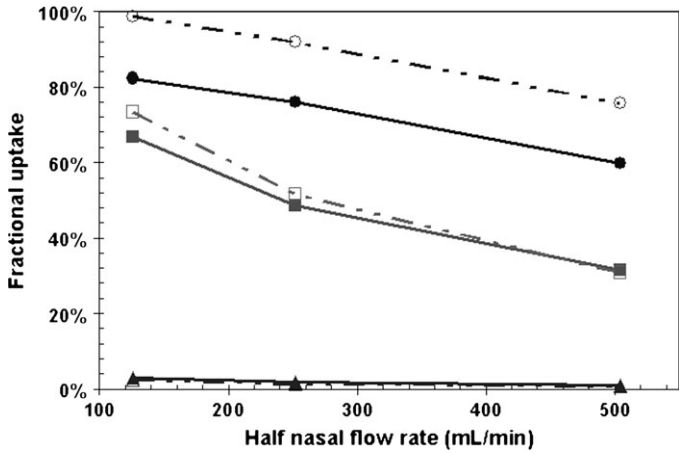

Figure 5 Fractional uptake η over the entire nasal surface plotted half-nasal flow rate $Q_{/2}$. Key: C (●/○), AC (■/□), octane (▲/Δ), inspiratory flow (solid lines), and expiratory flow (dashed lines).

Septal patterns of odorant uptake

Maximal absorption was predicted to take place on the upstream surfaces and shifted more downstream as the flow rate increased. This effect occurred for the simulation of both C (Figure 6) and AC uptake for both inspiratory and expiratory flow. As in the human nasal calculations done by Keyhani et al. (1997), low-solubility odorant uptake, such as for octane, is in general more sensitive to flow rate changes (Keyhani's Figure 15) than is uptake for high-solubility odorants, but this effect is also strongly dependent on nasal geometry. The low-solubility, high flow rate sensitivity effect can be seen in Figures 7B,C. In general, all simulated odorants exhibited less absorption in the lateral turbinate region on expiration than on inspiration because the steady flow S-shaped streamlines that ventilate this region on inspiration

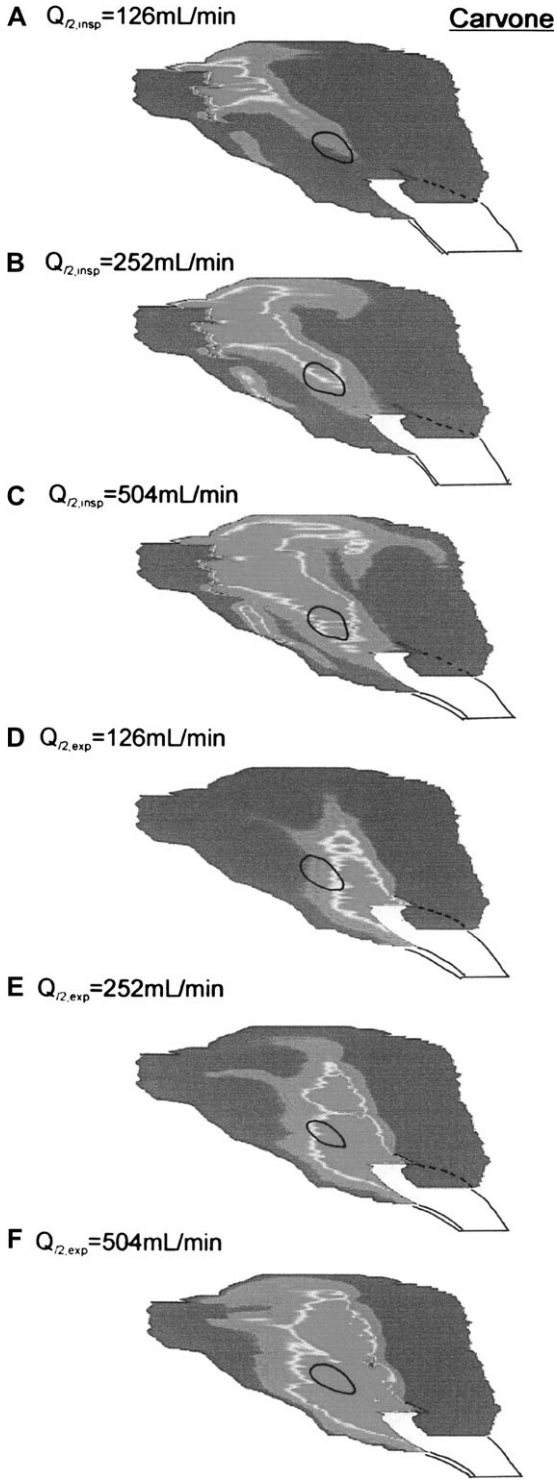

Figure 6 Contours of surface mass flux absorption of C on the right rat nasal cavity septal wall. Mass flux is normalized by the mass fraction at the external naris. The external naris is to the left and the nasopharyngeal meatus is to the right. **(A)** Inspiratory flow, $Q_{/2,insp}$ = 126 ml/min; **(B)** Inspiratory flow, $Q_{/2,insp}$ = 252 ml/min; **(C)** Inspiratory flow, $Q_{/2,insp}$ = 504 ml/min; **(D)** Expiratory flow, $Q_{/2,exp}$ = 126 ml/min; **(E)** Expiratory flow, $Q_{/2,exp}$ = 252 ml/min; and **(F)** Expiratory flow, $Q_{/2,exp}$ = 504 ml/min. The same scale is used for all plots, with 2.5×10^{-3} and 0 g/cm^2/s represented by the most extreme colors in the color spectrum — red and dark blue — respectively.

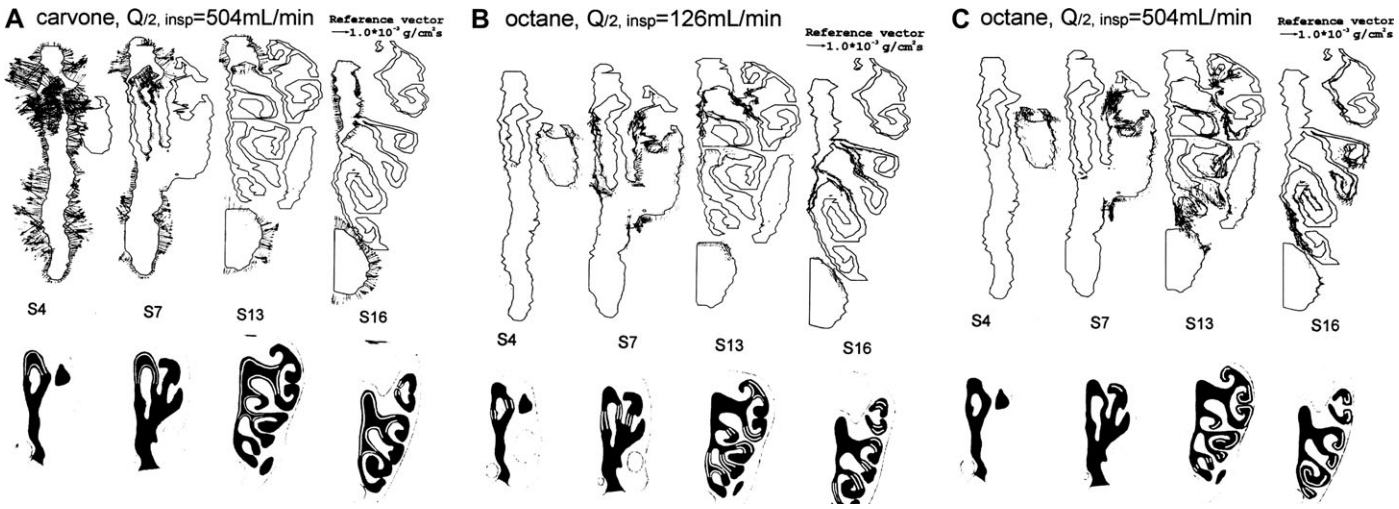

Figure 7 Comparison of surface mass flux vectors on the walls of 4 coronal sections (upper half figure) with the anatomic zones identified by Strotmann et al. (1994) shown as white lines on the edges of the black coronal sections in lower half figure. **(A)** C at $Q_{/2,insp}$ = 504 ml/min with dorsal zone (zone 1); **(B)** octane at $Q_{/2,insp}$ = 126 ml/min with medial zone (zone 2); and **(C)** octane at $Q_{/2,insp}$ = 504 ml/min with lateral zone (zone 3).

were much less prevalent on expiration (Yang 1999; Yang et al. 2006; Zhao et al. 2006).

Discussion

The numerical computations we have presented allow us to predict where on the rat nasal mucosa odorant molecules of varying solubilities will deposit.

Correlation of odorant surface absorption with anatomic zones

Several investigators have identified up to 4 biochemically distinct, neuroolfactory anatomical zones that are broad, circumscribed, and nonoverlapping and that extend anteroposteriorly throughout the olfactory epithelium in rodents (Ressler et al. 1993; Vassar et al. 1993; Strotmann et al. 1994; Sullivan et al. 1996). Serial coronal sections covering the entire olfactory epithelium were probed with a subtype-specific antisense RNA and analyzed to determine the spatial localization and the anteroposterior extent of expression zones for various receptor subtypes. The expression areas were defined as regions of olfactory epithelium with a minimum of 3 reactive cells and with boundaries at the last reactive cell. Every reactive area was found to have its symmetrical counterpart on the facing surface of the opposite turbinate. These zones have also been reported to be distributed with overlapping boundaries in some of the recent studies (Iwema et al. 2004; Miyamichi et al. 2005).

The results of our odorant uptake calculations suggest that there is a correlation between the local mass mucosal surface flux and some of the neuroolfactory anatomic zones in the rat nasal cavity described for specific receptor gene expression by Strotmann et al. (1994). We predicted that septal surface absorption of high- and medium-solubility odorants occurs in the dorsomedial region of the olfactory epithelium and that most absorption of low-solubility odorants occurs in the peripheral region of the olfactory epithelium along the anterior–posterior axis (see Figure 3A–F).

The regions of maximal highly soluble uptake correlated reasonably well with zone 1 (dorsal). AC was found to have a similar absorption pattern to C but with relatively smaller magnitude in mass surface flux. Octane (highly insoluble), on the other hand, was seen to be less absorbed in the zone 1 (dorsal) but more absorbed in the zone 2 (lateral) at low flow rate and in the zone 3 (ventral) at high flow rate.

Each anatomical receptor zone in theory contains receptors of the same type that are expressed in the presence of a certain group of odorants. The different zones (zone 1 and zones 2/3), corresponding to the uptake of 2 odorants of maximal difference in solubility (C and octane), represent 2 different topological anatomic regions that cover a large area of olfactory epithelium. Solubility is the major numerical modeling parameter that results in this regional uptake difference. Future investigation of odorants with intermediate solubilities, variations in mucus thickness, and fully unsteady airflow may add to our understanding of the correlation between the receptor zones and odorant solubility.

Recently, Schoenfeld et al. (Schoenfeld and Knott 2002, 2004; Schoenfeld and Cleland 2006) have postulated the existence of a ''Fovea'' in the hamster nose by noting a disproportionate mapping of olfactory neurons in the olfactory epithelium onto target cells in the main olfactory bulb. They postulated that the large difference they observed in central and peripheral (medial and lateral) air channel innervation could be exploited by the hamster for odorant detection—again an example of the optimization of imposed and inherent patterning similar to our results for C and octane.

Comparison of odorant surface absorption with electroolfactogram recordings

Scott et al. (Ezeh et al. 1995; Scott et al. 1996, 1997, 2000; Scott and Brierley 1999) made observations in electroolfactogram recordings from the rat nose showing a general alignment with the expression zones. They (Ezeh et al. 1995; Scott et al. 1996, 1997) suggested, in general, that odorants lacking oxygen-containing functional groups (relatively insoluble in mucus) evoked larger responses in the lateral sites and that odorants containing ketone groups (relatively more soluble in mucus) evoked larger dorsomedial responses. For example, as shown in Table 2, octane (straight chain alkane—lacking oxygen and insoluble in mucus) would be expected to produce a larger lateral response, whereas C (a ketone—containing oxygen and very soluble in mucus) and AC (containing oxygen and also relatively soluble in mucus) would be expected to produce larger dorsomedial responses.

Our results, which are dependent on odorant mucus solubility, are in general agreement with their findings. C and AC were both predicted to be absorbed dorsomedially, whereas octane was predicted to be preferentially absorbed laterally. This is true for all 3 different flow rates during both inspiratory and expiratory flow.

Uptake along the S-shaped streamline path

From velocity field modeling of airflow in the rat nasal cavity (Kimbell et al. 1997; Yang 1999; Yang et al. 2006; Zhao et al. 2006), some inspiratory streams, originating from the dorsal side of the anterior nose, appear to take more circuitous S-shaped routes through the olfactory region than straightforward flow paths. These simulated streams enter the convoluted ethmoid recesses, then reverse and bend backward toward the external naris, and finally exit through the dorsal region of the nasopharyngeal meatus. This reverse flow is identified for all 3 different flow rates in steady inspiratory flow but is much less prevalent during steady expiratory flow, especially for higher flow rates.

In the present study, absorption of C and AC during inspiratory flow was predicted to take place preferentially on the olfactory epithelium in the dorsomedial region along the path of the S-shaped streamlines. During expiratory flow, simulations predicted that olfactory epithelium in the dorsomedial region did not experience high surface flux for these odorants because the reverse flowing S-shaped streamlines were much fewer—see Figure 3A–C. Octane also traveled along the S-shaped streamlines in simulations but was absorbed more laterally in the olfactory region because it was not appreciably absorbed upstream before reaching these sites—see Figure 3E–F.

Comparison of odorant uptake during inspiratory and expiratory flow

Simulations predicted that different odorant uptake patterns exist for inspiratory and expiratory flow. Higher absorption generally takes place on the upstream surface for all 3 odorants with the effect shown most prominently for highly soluble C (Figure 6). For example, peak flux was predicted to occur in the anterior nose during inspiratory flow, whereas for expiration, it was predicted to lie near the turbinate bone around the top end of nasopharyngeal meatus at the opening of the septal window.

Vector plots of the mass surface flux on the 4 coronal planes also showed different absorption patterns for opposite flow directions. Interpretation of the plots however requires caution. Because the inlet concentration boundary condition for expiratory flow was normalized to be $c = 1.0$, the vector plots for expiratory flow showed larger upstream odorant uptake because the 4 coronal sections were located more upstream in the flow path during expiratory flow. In future studies, the effect of odorant absorption in the lower respiratory airways needs to be included in the expiratory concentration inlet condition—see also comment below.

In general, it was predicted that less odorant flow ran through the olfactory region during expiration than inspiration because the S-shaped streamlines were less prevalent and odorant absorption in the lower lung airways would have occurred. Also, less odorant absorption was predicted to occur laterally on expiration, and therefore less odorant exposure to the zones 2 and 3 was predicted on expiration than on inspiration. It is possible that these inspiratory and expiratory flux differences are exploited by the rat when using its high frequency sniffing strategy (Youngentob et al. 1987) to aid in odor detection.

As the expiration model in this study was based on release of odorant molecules from the nasopharyngeal meatus, there may be concerns that molecules of certain odorants, that is, strongly absorbed C, would never start their expiratory migration from nasopharyngeal meatus but rather from the place to which they had migrated at the end of the inspiratory phase of the sniff cycle. Because the mathematical model is linear, the amount of odorants entering at the initial location will not affect the fraction deposited downstream or the sites where deposition occurs. It is true that much less odorants will enter the nasopharynx on expiration if the lower airways are fully modeled, but the pattern and site of expiratory nasal cavity deposition will be unchanged. It is the pattern and the location of odorant deposition that are most important in this study and in olfaction in general.

Effect of flow rate on absorption magnitude

Absolute response magnitude for C was found to increase with flow rate for constant inlet odorant concentration in the voltage-sensitive dye measurements recorded by Kent et al. (1996). In contrast to the more strongly absorbed C, the responses to weakly absorbed propyl acetate displayed little gradient in response magnitude along the flow path and, as flow rate increased, the pixel-by-pixel response magnitudes decreased.

Our results generally agree with those of Kent et al. The residence time of odorant molecules at a given region above the nasal mucosa is decreased as the flow rate increases. Therefore, for a weakly soluble odorant, the response magnitude at those 4 coronal cross sections decreases as the flow rate increases. However, for a highly soluble odorant (such as C), increasing flow rate reduces much of the upstream absorption and allows a greater number of molecules to reach downstream locations. Consequently, for a highly soluble odorant, the response magnitude at the 4 coronal cross sections increases as the flow rate increases.

Effect of flow rate on location of uptake

The effect of flow rate for constant inlet odorant concentration on the location of high surface flux absorption was explored by studying the shift of predicted high flux regions while varying the inspiratory flow rate. With the low inspiratory flow rate (126 ml/min), octane (very insoluble) was predicted to be preferentially absorbed in the surface receptor region (Figure 7B) that roughly correlates to the medial zone 2. The region of maximal absorption for octane, however, was predicted to shift to the lateral zone 3 (Figure 7C) with the high inspiratory flow rate (504 ml/min). No obvious zone shifting due to flow rate increase can be identified for the more soluble C (Figure 7A) and AC absorption during inspiratory flow.

Effect of flow rate on total flux and absorption efficiency

Total odorant surface flux normalized by the odorant ambient mass fraction over the entire nasal surface was predicted to increase (absorption of a gas of the density of air for both inspiratory and expiratory flow) as half-nasal flow rate increases (see Figure 4). For a given odorant concentration, the convective flow at the inlet increases as flow rate increases, and consequently the thickness of the concentration boundary layer in the developing regions of the flow decreases. Therefore, total mass surface flux of all 3 odorants increases as expected for constant inlet odorant concentration.

The fractional uptake, η, over the entire nasal surface for all 3 odorants, however, was predicted to decrease as the flow rate increases (Figure 5). This is due to a decrease in residence time of odorant molecules in the nasal cavity as flow rate increases. It should be noted that the fractional uptake shown in Figure 5 is proportional to the total nasal odorant surface deposition obtained when the number of incoming odorant molecules is held constant. The latter can be obtained by multiplying all points on the curve in Figure 5 by the constant mass of odorant inhaled. During expiration, fractional uptake was predicted to be greater than on inspiration. This slight difference could be due to the inlet velocity and concentration profiles assumed in our calculations.

Youngentob et al. (1987) postulated that in order to facilitate the arrival of odorant molecules at the olfactory receptors, one of the possible mechanisms in rat sniffing strategy may be to minimize the number of molecules absorbed in nonolfactory tissue. Our findings on the flow rate effect generally agreed with this suggestion. The relative lack of lateral olfactory flow on expiration means that odorant molecules that have entered this region on inspiration will not be washed out from it on expiration. Expiratory flow at very low flow rate (as is present at the beginning of expiration) may indeed wash out some of the olfactory recesses. This remains to be investigated by doing time-dependent (fully unsteady) flow simulations in the rat nose over the whole cycle of inspiration and expiration.

Concluding remarks

We developed an anatomically accurate 3D numerical model of the right nasal cavity of the Sprague-Dawley rat and used it to compute the location of the mucosal uptake of 3 odorants of widely differing mucosal solubility. We studied the imposed mucosal patterning of these odorants during high, medium, and low flow rates for both inspiratory and expiratory flow. We predicted that odorants highly soluble in mucus were absorbed dorsally and medially corresponding roughly to receptors of zone 1 (dorsal). Simulated insoluble odorants tended to be absorbed more ventrally and laterally in the rat olfactory region corresponding to zones 2 and 3 (medial and lateral). These findings also agreed with the electroolfactogram measurements of Scott et al. (Ezeh et al. 1995; Scott et al. 1996, 1997), the enzyme histochemistry measurements of Schoenfeld et al. (Schoenfeld and Knott 2002, 2004; Schoenfeld and Cleland 2006), and the voltage-sensitive dye measurements of Kent et al. (1992, 1996). This numerical approach is the first to provide detailed odorant flux information across the olfactory mucosa in the rat nasal cavity during inspiratory and expiratory flow and to relate anatomic olfactory receptor location, physiological function, and biochemical experiment to numerical odorant flow and transport data. This numerical technique can allow us to separate the contributions of imposed and inherent patterning mechanisms on the rat olfactory mucosa and contribute to our deeper understanding of olfaction.

Appendix

List of symbols

c: nondimensional odorant mass concentration (in air) (nondimensionalized by the inlet odorant concentration C_0).
C_0: odorant mass concentration at the external naris.
u: air velocity vector.
d_{in}: hydraulic diameter (= 4 × area/perimeter) of the external naris.
D_m: diffusivity of inhaled odorant in the mucus phase.
D_a: diffusivity of inhaled odorant in the air phase.
β: odorant partition coefficient at the air–mucus interface $\left(c_a|_{y=0} = \beta c_m|_{y=0}\right)$.
H_m: thickness of the mucus layer.
N_{St}: Strouhal number (=$\omega L/U_{in}$).

N_{Re}: Reynolds number ($=U_{in}d_{in}/\nu$).
N_{Sc}: Schmidt number ($=\nu/D_a$).
K: nondimensional wall surface parameter ($=(d_{in}D_m)/(D_a\beta H_m)$).
ν: kinematic viscosity of air.
ρ: density of air.
j_n: flux vector ($=-D_a\partial c_a/\partial y|_{wall}$; g/cm^2/s).
J: total odorant mass flow over a given wall surface area (g/s).
A: total surface area (cm^2).
η: absorption efficiency (or fractional uptake) over the entire nasal surface.
$Q_{/2}$: half-nasal flow rate (insp or exp for inspiratory or expiratory flow).
y: coordinate normal to the nasal epithelium surface.
L: axial length of nasal cavity.
U_{in}: average velocity over a given cross section.
ω: angular breathing frequency.

Acknowledgements

The authors appreciate the comments of the reviewers on the manuscript. This work was supported by the National Institute of Deafness and Other Communication Disorders grant NIDCD-00072.

References

Adrian ED. 1950. Sensory discrimination with some recent evidence from the olfactory organ. Br Med Bull. 6:330–331.

Ezeh PI, Davis LM, Scott JW. 1995. Regional distribution of rat electroolfactogram. J Neurophysiol. 73(6):2207–2220.

Getchell TV, Margolis TV, Getchell ML. 1984. Perireceptor and receptor events in vertebrate olfaction. Prog Neurobiol. 23:317–345.

Hornung DE, Mozell MM. 1981. Accessibility of odorant molecules to the receptors. In: Cagan RH, Kare MR, editors. Biochemistry of taste and olfaction. New York: Academic Press. p. 33–45.

Hornung DE, Mozell MM, Serio JA. 1980. Olfactory mucus/air partitioning of odorant. In: van der Starre H, editor. Olfaction and taste VII. London (UK): IRL Press. p. 167–170.

Hornung DE, Youngentob SL, Mozell MM. 1987. Olfactory mucosa/air partitioning of odorants. Brain Res. 413:147–154.

Howard PH, Meylan WM, Fake FF. 1997. Handbook of physical properties of organic chemicals. 1st ed. Boca Raton (FL): CRC Press/Lewis Publishers.

Iwema CI, Fang H, Kurtz DB, Youngentob SL, Schwob JE. 2004. Odorant receptor expression patterns are restored in lesion-recovered rat olfactory epithelium. J Neurosci. 24:356–369.

Kauer JS, Moulton DG. 1974. Responses of olfactory bulb neurones to odor stimulation of small nasal areas in the salamander. J Physiol. 243: 717–737.

Kent PF, Mozell MM. 1992. The recording of odorant-induced mucosal activity patterns with a voltage-sensitive dye. J Neurophysiol. 68: 1804–1819.

Kent PF, Mozell MM, Murphy SJ, Hornung DE. 1996. The interaction of imposed and inherent olfactory mucosal activity patterns and their composite representation in a mammalian species using voltage-sensitive dyes. J Neurosci. 16:345–353.

Keyhani K, Scherer PW, Mozell MM. 1997. A numerical model of nasal odorant transport for the analysis of human olfaction. J Theor Biol. 186: 279–301.

Kimbell JS, Godo MN, Gross EA, Joyner DR, Richardson RB, Morgan KT. 1997. Computer simulation of inspiratory airflow in all regions of the F344 rat nasal passages. Toxicol Appl Pharmacol. 145:388–398.

Mackay-Sim A, Shaman P, Moulton DG. 1982. Topographic coding of olfactory quality: patterns of epithelial responsivity in the salamander. J Neurophysiol. 48:584–596.

Miyamichi K, Serizawa S, Kimura HM, Sakano H. 2005. Continuous and overlapping expression domains of odorant receptor genes in the olfactory epithelium determine the dorsal/ventral positioning of glomeruli in the olfactory bulb. J Neurosci. 25:3586–3592.

Moulton DG. 1976. Spatial patterning response to odors in the peripheral olfactory system. Physiol Rev. 56:578–593.

Mozell MM, Kent PF, Murphy SJ. 1991. The effect of flow rate upon the magnitude of the olfactory response differs for different odorants. Chem Senses. 16:631–649.

Mozell MM, Sheehe PR, Hornung DE, Kent PF, Youngentob SL, Murphy SJ. 1987. "Imposed" and "inherent" mucosal activity patterns. J Gen Physiol. 90:625–650.

Ressler KJ, Sullivan SL, Buck LB. 1993. A zonal organization of odorant receptor gene expression in the olfactory epithelium. Cell. 73:597–609.

Schoenfeld TA, Cleland TA. 2006. Anatomical contributions to odorant sampling and representation in rodents: zoning in on sniffing behavior. Chem Senses. 31:131–144.

Schoenfeld TA, Knott TK. 2002. NADPH diaphorase activity in olfactory receptor neurons and their axons conforms to a rhinotopically-distinct dorsal zone of the hamster nasal cavity and main olfactory bulb. J Chem Neuroanat. 24:269–285.

Schoenfeld TA, Knott TK. 2004. Evidence for the disproportionate mapping of olfactory airspace onto the main olfactory bulb of the hamster. J Comp Neurol. 476:186–201.

Scott JW, Brierley T. 1999. A functional map in rat olfactory epithelium. Chem Senses. 24:679–690.

Scott JW, Brierley T, Schmidt FH. 2000. Chemical determinants of the rat electro-olfactogram. J Neurosci. 20:4721–4731.

Scott JW, Davis LM, Shannon D, Kaplan C. 1996. Relation of chemical structure to spatial distribution of sensory responses in rat olfactory epithelium. J Neurophysiol. 75:2036–2049.

Scott JW, Shannon DE, Charpentier J, Davis LM, Kaplan C. 1997. Spatially organized response zones in rat olfactory epithelium. J Neurophysiol. 77:1950–1962.

Strotmann J, Wanner I, Helfrich T, Beck A, Breer H. 1994. Rostro-caudal patterning of receptor-expressing olfactory neurones in the rat nasal cavity. Cell Tissue Res. 278:11–20.

Sullivan SL, Adamson MC, Ressler KJ, Kozak CA, Buck LB. 1996. The chromosomal distribution of mouse odorant receptor genes. Proc Natl Acad Sci USA. 93:884–888.

Vassar R, Ngai J, Axel R. 1993. Spatial segregation of odorant receptor expression in the mammalian olfactory epithelium. Cell. 74: 309–318.

Welty JR, Wicks GE, Wilson RE. 1976. Fundamentals of momentum, heat and mass transfer. 2nd ed. Wiley, New York.

Yang CC. 1999. Numerical modeling of odorant uptake in the rat and bullfrog nasal cavities [dissertation]. [Philadelphia (PA)]: University of Pennsylvania.

Yang GC, Scherer PW, Mozell MM. 2006. Modeling Inspiratory and Expiratory Steady-State Velocity Fields in the Sprague-Dawley Rat Nasal Cavity. Chem Senses. doi:10.1093/chemse/bjl047.

Youngentob SL, Mozell MM, Sheehe PR, Hornung DE. 1987. A quantitative analysis of sniffing strategies in rats performing odor detection tasks. Physiol Behav. 41:59–69.

Zhao K, Dalton P, Yang GC, Scherer PW. 2006. Numerical modeling of turbulent and laminar airflow and odorant transport during sniffing in the human and rat nose. Chem Senses. 31(2):107–118.

Zhao K, Scherer PW, Hajiloo SA, Dalton P. 2004. Effect of anatomy on human nasal air flow and odorant transport patterns: implications for olfaction. Chem Senses. 29:365–379.

Accepted December 15, 2006